Research Square

Preprints are preliminary reports that have not undergone peer review.
They should not be considered conclusive, used to inform clinical practice,
or referenced by the media as validated information.

PI3Kδ is selectively inhibited by roginolisib through stabilizing of the C-terminal helix kα12

Gerhard Hummer

gerhard.hummer@biophys.mpg.de

Max Planck Institute of Biophysics https://orcid.org/0000-0001-7768-746X

Oscar Vadas

University of Geneva https://orcid.org/0000-0003-3511-6479

Simon Tiede

Max Planck Institute for Biophysics https://orcid.org/0009-0001-1712-5454

Maria Chaouki

Centre de Recherches en Cancérologie de Toulouse

Laura Tesmer

Max Planck Institute for Biophysics

Shanlin Rao

University of Cambridge https://orcid.org/0000-0003-4892-5523

Rémy Visentin

University of Geneva https://orcid.org/0000-0002-4022-7045

Ulrich Graedler

Discovery Technologies, Merck KGaA, Frankfurter Straße 250, 64293 Darmstadt

Martin Augustin

Proteros biostructures GmbH

Rainer Kiefersauer

Proteros biostructures GmbH

Carola Gößer

Proteros biostructures GmbH

Anne Quillet-Mary

UMR1037 Inserm-Univ. Toulouse III Paul Sabatier-UMR 5071CNRS https://orcid.org/0000-0002-1849-6388

Loic Ysebaert

CRCT

Julie Guillermet-Guibert

INSERM U1037, CRCT, Université de Toulouse, F-31037 Toulouse, France https://orcid.org/0000-0003-3173-4907

Lars van der Veen

iOnctura SA

Giusy Di Conza

iOnctura SA https://orcid.org/0000-0003-1353-5867

Article

Keywords:

Posted Date: January 7th, 2026

DOI: https://doi.org/10.21203/rs.3.rs-8048396/v1

License: This work is licensed under a Creative Commons Attribution 4.0 International License. Read Full License

Additional Declarations: Yes there is potential Competing Interest. Some authors (as listed) are employees of the study Sponsor (iOnctura) with stock options.

Version of Record: A version of this preprint was published at Nature Communications on October 9th, 2026. See the published version at https://doi.org/10.1038/s41467-026-77424-0.

Abstract

Phosphoinositide 3-kinases (PI3Ks) are major regulators of cell growth, proliferation and signalling, constituting key therapeutic targets in cancer, inflammation, and other diseases. Individual class I PI3K isoforms control key cellular functions, imposing the need to generate isoform-specific inhibition for therapeutic intervention. Roginolisib is a selective PI3Kδ inhibitor that shows promise for the treatment of cancer. Using a combination of X-ray crystallography, molecular dynamics simulations, and hydrogen-deuterium exchange mass spectrometry, we have uncovered the mechanism driving roginolisib's potent and isoform-selective inhibition of PI3Kδ. Roginolisib uniquely stabilises the catalytic C-terminal helix kα12, locking the enzyme in an inactive conformation. This binding mode also results in more sustained inhibition of phosphatidylinositol 3,4,5-trisphosphate formation in tumour samples of CLL patients. Inhibition of PI3Ks by stabilization into an inactive conformation has not been described before and may provide the basis for novel, more selective and effective pharmacological strategies.

Introduction

Phosphoinositide 3-kinases (PI3Ks) are lipid-modifying enzymes that phosphorylate the 3'-hydroxyl group of inositol phospholipids. They are involved in a number of physiological processes crucial for cell survival, growth, and differentiation [1]. Class I PI3Ks are receptor-activated heterodimeric enzymes that are composed of a catalytic and a regulatory subunit. They convert phosphatidylinositol-4,5-bisphosphate (PIP2), which is mainly found at the intracytoplasmic face of the cell membrane, into phosphatidylinositol-3,4,5-trisphosphate (PIP3). The class IA catalytic subunits p110α, p110β, and p110δ are associated with p85 regulatory subunits and mediate stimulation downstream of receptor-tyrosine kinases (RTKs) and G protein-coupled receptors (GPCRs) [2]. The only Class IB catalytic subunit, p110γ, forms heterodimers with p84 or p101 regulatory subunits, mediating signals downstream of GPCRs. Activation of the kinase Akt through PIP3 leads to downstream processes that include inhibition of apoptosis and activation of protein synthesis. The PI3K pathway is among the most frequently activated in human cancer [3], making the different isoforms attractive pharmacological targets for development of isoform-specific inhibitors [4].

The catalytic subunit of the PI3Kδ isoform, p110δ, is encoded by the PIK3CD gene [5] and in contrast to the other class IA PI3Ks, p110α and p110β, p110δ is preferentially expressed within immune cells [6]. PI3Kδ signaling regulates activation and differentiation of immune cells [7], and inactivation of PI3Kδ has been shown to impact the function of T cells, B cells, mast cells and neutrophils [1]. Based on the pivotal role of PI3Kδ for the development and expansion of malignant B-cells, several PI3Kδ inhibitors have been developed [8].

Idelalisib (Zydelig) was the first PI3Kδ inhibitor developed for the treatment of B-cell malignancies. Its efficacy has been demonstrated in several clinical studies, resulting in its approval by the United States Food and Drug Administration for treatment of patients with relapsed chronic lymphocytic leukaemia

(CLL) and indolent non-Hodgkin lymphoma (NHL) [9]. Unfortunately, idelalisib and similar first generation PI3Kδ inhibitors have been associated with variable degrees of toxicity, ultimately leading to withdrawal of the accelerated approvals received for their use in NHL [10].

The factors responsible for the toxicity of these first-generation inhibitors are not fully understood. However, insufficient isoform selectivity is likely a major contributor [11,12]. Achieving high selectivity among PI3K isoforms remains challenging due to the conserved catalytic site. Targeting regions away from the ATP binding pocket, for example using allosteric modulators, holds promise [13]. In addition, the complex regulatory mechanisms controlling PI3K activation provide opportunities to interfere with kinase activity “at a distance” and possibly, with enhanced isoform selectivity [14].

PI3Kδ is autoinhibited by reversible inhibitory contacts of the nSH2- and cSH2 domains of the p85 regulatory subunit with the C2, helical and kinase domain of p110δ [14–16]. Localization of PI3Kδ to the membrane is promoted by Ras binding to the Ras binding domain (RBD) of p110δ [17] and at the membrane PI3Kδ is activated by phosphorylated tyrosine (pY) motifs of RTKs that have high affinity binding to the p85 nSH2/cSH2 domains, releasing their autoinhibitory activity. For full activation of PI3Kδ at the membrane, a conformational change is also required in the regulatory arch spanning the p110δ catalytic domain involving helices kα10, kα11 and kα12, which must change from a closed to an open state [14,17]. Each of these steps towards full activation of the kinase and the conformational changes involved may offer opportunities for specific inhibition.

Roginolisib is a novel, small molecule inhibitor, that selectively targets the PI3Kδ isoform and is currently evaluated in Phase II trials. It was investigated in a first-in-human (FIH) dose study, where it showed a favourable metabolic and pharmacokinetic profile, resulting in high target specificity and a promising safety profile, distinguishing it from first generation PI3Kδ inhibitors [12,18]. Unlike idelalisib, roginolisib has been shown to retain its potency, even at high ATP concentrations [19]. We therefore hypothesized that the binding mode of roginolisib to PI3Kδ might be unique, potentially accounting for its distinct safety profile observed in the clinic. To understand how this drug achieves high isoform selectivity, we aimed to investigate the differences in PI3Kδ binding interactions between roginolisib and idelalisib, using a combination of X-ray crystal structure analysis, molecular dynamics (MD) simulations, and hydrogen-deuterium exchange mass spectrometry (HDX-MS). Additionally, we explored potential differences in the inhibition of PIP3 formation in CLL patient samples. We identified a novel inhibitor binding mode to PI3Kδ that induces conformational changes and locks the kinase into an inactive state, leading to a more efficacious inhibition of PIP3 formation. Strong interactions with isoform-specific regulatory elements at the C-terminus may explain the comparably high selectivity of the inhibitor.

Results

X-ray crystal structures reveal distinct binding modes of roginolisib and idelalisib

In order to elucidate the differences in PI3Kδ binding interactions between roginolisib and idelalisib we investigated the co-crystal structure of the roginolisib-PI3Kδ complex at 2.75 Å resolution (PDB-ID: 9T07, Fig. 1a and b and supplementary Fig. S1). The solved crystal structure revealed complete electron density for roginolisib within the ATP pocket and indicates an H-bond contact between the morpholine O-atom and the backbone NH of Val828, which belongs to the hinge region. In addition, roginolisib forms π-stacking interactions via the pyrazole ring to Trp760 and extensive van-der-Waals (vdW) contacts to Met752, Pro758, Ile777, Tyr813, Ile825, Thr833, Met900 and Phe908 [20].

The binding modes of roginolisib and idelalisib (Fig. 1c) are markedly different. Whereas both inhibitors form a hydrogen bond (3.0 and 2.9 Å distance, respectively) to Val828 in the hinge region of the ATP pocket, roginolisib does not occupy the so called PI3Kδ “specificity” pocket at the interface between the side chains of Met752, Pro758, Trp760 and Ile777 [21]. Instead, roginolisib engages the Met752 and Trp760 residues that shape the specificity pocket in vdW and π-π-interactions, reorienting the sidechains, compared to the complex with idelalisib. Furthermore, the sulfoxide in the core structure of roginolisib forms a hydrogen bond to Lys779 (3.1 Å distance) and the aromatic fluorine-atom a fluor hydrogen bond (2.9 Å distance) to Ser754, both residues not addressed by idelalisib. Another notable difference is that Asp897 forms a strong (2.6 Å distance) hydrogen bond with His895 of the DRH motif in the roginolisib structure, whereas in the idelalisib structure His895 forms a hydrogen bond (3.3 Å distance) with Asp893. Also, both inhibitors interact differently with Asp911 and. The carboxamide of roginolisib is part of a hydrogen bonding network involving a water molecule in the ATP pocket and the backbone NH of Asp911 (Fig. 1b). This water molecule is also engaged by the core imidazopyrimidine structure of idelalisib, however, the second hydrogen bond is formed with the side chain carboxylate of Asp911 and not with its backbone NH (Fig. 1.c).

As part of the conserved DFG motif within the kinase activation loop, Asp911 is expected to coordinate the magnesium ion in kinases [22,23]. The distinction between a “DFG-in” and “DFG-out” conformation has been reported to influence ligand selectivity and binding affinity [24]. In the DFG-in conformation, the aspartate is oriented towards the active site with the phenylalanine in the opposite direction, whereas the orientation of the two residues is reversed in the DFG-out conformation [25,26]. While no apparent difference was observed in the phenylalanine orientation, the DFG motif’s aspartate adopted alternative conformations in the presence of roginolisib or idelalisib, respectively (Fig. 1c, supplementary Fig. S2). The binding of roginolisib pushes Asp911 into a DFG-in-like configuration. In contrast, idelalisib leaves the residue in a rotated (by 90°) orientation resembling the DFG-out aspartate conformation.

To confirm if the observed differences in binding interactions between idelalisib and roginolisib are consistent, the co-crystal structure of PI3Kδ in complex with a close analogue of roginolisib, IOA-288, was solved at 2.97 Å resolution (PDB-ID: 9T1P, supplementary Fig. S1 and S3). In this crystal structure IOA-288 shows identical binding interactions to roginolisib with the difference that the Asp911 is tilted even further inward. In addition, the side chain conformations of Met752 and Trp760 are slightly

modified to adopt IOA-288's second morpholine ring, which is in vdW contacts with both residues (Fig. S3).

Molecular dynamics simulations show that roginolisib reorients catalytic kα11/kα12 helices towards the active site

A major limitation of the roginolisib and IOA-288 crystal structures is the fact that only the catalytic p110δ subunit and the p85α iSH2 domain were crystallized and no electron density was obtained for the C-terminal kα12 helix. This has also been the case with other published co-crystal structures of inhibitor-bound PI3Kδ. To investigate the impact of the different inhibitor binding modes on the conformation and dynamics of the p110δ C-terminal region, we modelled the unresolved protein regions based on structural prediction by Alphafold [27]. To validate the modelled full-length p110δ structure, we compared it to the p110β/p85β-icSH2 crystal structure (PDB-ID: 2Y3A, Fig S4), for which the kα12 helix has been partially resolved in its inactive conformation [28]. The modelled p110δ kα12 helix proved to align well, suggesting that the full-length p110δ model also represents an inactive protein conformation (Fig. S4). All-atom MD simulations were conducted on full-length p110δ bound to either roginolisib, idelalisib, or ATP. These simulations confirmed stable binding of all three molecules within the ATP pocket of PI3Kδ (Fig. S5). The key hydrogen-bond interactions with Val828 (idelalisib and roginolisib) and Lys779 (roginolisib) were also confirmed.

Surprisingly, consistent differences were observed in the conformational dynamics of the C-terminus between the different ligand-bound states, across five replicate simulations of each structure (Fig. 2a). In the ATP-bound form of the protein, the C-terminal helix kα12 remained stable in its initial orientation relative to kα11. However, in the presence of the two inhibitors the angle between the two helices exhibited distinct shifts (Fig. 2b). In multiple simulation replicates (2–5 μs in length) of the roginolisib-bound protein, kα12 further levered towards the kinase active site. The C-terminal half of kα12 showed unfolding whereas the N-terminal half maintained its α-helical secondary structure. In clear contrast, kα12 levered away from the idelalisib-bound protein, ultimately resulting in a ~ 35° difference between the most probable kα11-kα12 angle of the roginolisib- and idelalisib-bound state (Fig. 2b). The simulated effect of roginolisib on helix kα12 is consistent with the reported auto-inhibitory role of the C-terminus in the absence of lipid substrate, whereby kα12 was proposed to impede ATP hydrolysis by folding over the active site [15,29,30]. With membrane association of kα12 and its concomitant repositioning proposed to be required for PI3K activation [30–32], the inhibitory effect of roginolisib may stem from its ability to promote a pronounced bend of the kα11/kα12 configuration, sequestering kα12 away from substrate binding at the membrane.

Examination of the simulated ligand-bound p110δ structures revealed that two basic residues within helix kα12, Lys1040 and Arg1043, formed distinct contacts in the presence of different bound ligands. In the ATP-bound protein, Lys1040 and Arg1043 interacted with the γ-phosphate of ATP, likely with a stabilising effect on ATP binding, and these interactions may play a role in the process of PIP2

phosphorylation. The magnesium ion was coordinated by Asp911 of the DFG motif forming part of the kinase activation loop (Fig. 3a).

In the presence of roginolisib, Asp911 was pushed sterically into proximity with Asp897 (Fig. 3b) to form a negatively charged cluster. Both aspartate residues maintained strong electrostatic interactions with one or both basic kα12 residues Lys1040 and Arg1043 (Fig. 3c). This led to stabilisation of the protein conformation with helix kα12 close to the active site. By contrast, in the presence of idelalisib Asp911 pointed away from Asp897, and no aspartate cluster was formed. Arg1043 was in sporadic contact with Asp897 in the idelalisib-bound state, whilst neither Lys1040 nor Asp911 formed any considerable interactions. Lys1040 was oriented towards the solvent for most of each simulation replicate (Fig. 3b).

Hydrogen/deuterium exchange mass spectrometry analysis of heterodimeric p110δ/p85α confirms stabilisation of the C-terminal kα12 helix upon roginolisib binding

To follow up on the prediction that roginolisib affects the kα12 helix conformation, we set out to study the dynamics of full-length p110δ/p85α upon inhibitor binding, in solution. We turned to HDX-MS which has previously shown its strength for studying PI3Ks structures [15,31,33]. Recombinant human PI3Kδ (p110δ/p85α) produced from insect cells was used and three different deuterium labelling conditions were compared to identify potential conformational changes upon inhibitor binding: i) PI3Kδ, ii) PI3Kδ + roginolisib, and iii) PI3Kδ + idelalisib. From a total of 283 peptides encompassing the p110δ subunit, four regions showed differential H/D exchange rates upon inhibitor binding (Fig. 4a, Fig. S6, Tables S3-5). Most of the protein remained unchanged, highlighting the minimal impact of inhibitor binding on overall PI3Kδ conformation. As expected, binding of roginolisib and idelalisib each protected the hinge region from H/D exchange (827–836) confirming their binding to the ATP site. In addition, both compounds similarly deprotected region 698–713, which contains the loop between helix kα1-kα2 in the kinase domain, a region involved in membrane interaction (Fig. 4b and c) [15]. This modification highlights a conformational change of a loop distant from the inhibitor binding site, which may contribute to the inhibitory mechanism of these compounds. Uniquely, binding of roginolisib protects the C-terminal helix kα12 from H/D exchange (region 1022–1044), indicating either direct interaction with this region, and/or stabilisation of the secondary structure (Fig. 4a, c). Identification of this protection is in agreement with the folding of kα12 over the active site and thus supports the results of the MD simulation and a different mode of inhibition between roginolisib and idelalisib.

Roginolisib and idelalisib share a similar binding mode to the activated PI3Kδ heterodimer

The differential mode of binding between roginolisib and idelalisib observed by both MD simulations on p110δ and experimental HDX-MS on p110δ/p85α heterodimer, suggests that roginolisib may target the inactive state. To test this hypothesis, we generated a partially activated PI3Kδ heterodimer by inserting a mutation in the regulatory subunit that releases the p85α-cSH2 inhibitory contact [15,28]. The residue Y685 on p85α has been shown to mediate the inhibitory contact of the cSH2 domain with the elbow region connecting helices kα11 and kα12 of p110δ [15]. By replacing the tyrosine for alanine, the p85α-

Y685A mutation results in enhanced catalytic activity of p110δ via the loss of cSH2-mediated inhibition. HDX-MS analysis confirmed that the p85α-Y685A mutation exposes the C-terminal kα11-kα12 helices of p110δ, together with the end of the substrate binding loop 927–940 lying just beneath the elbow and the closely-located 855–868 loop (Fig. 5a-c) [15].

Binding of idelalisib to the p85α-Y685 PI3Kδ affected the same regions as in the WT heterodimer, indicating a similar binding mode between the activated and inhibited states (Fig. 4a, Fig. 5d). The situation differs for roginolisib, where protection of the kα12 helix (1022–1044) was only seen for the WT enzyme (Fig. 4a, Fig. 5d). This suggests that roginolisib, in contrast to idelalisib, makes additional contacts with the C-terminal region of the inactive kinase, which are lost upon activation of PI3Kδ. As both membrane binding and p85α-cSH2 contact release lead to conformational rearrangements of the catalytic domain, these experiments suggest that roginolisib preferentially targets the inactive enzyme and, by limiting kα12 conformation flexibility, prevents its activation.

Roginolisib's binding mode involving kα12 interactions is selective for the delta isoform

Despite their conserved structures, sequence variations between PI3Ks present opportunities for isoform-selective targeting by pharmacological agents. Within the C-terminal kα12 helix, the two key residues identified above, Lys1040 and Arg1043, are unique to the δ and β isoforms Fig. S7a). Given that these residues appear to be involved in roginolisib's binding to the kinase, a mechanistic rationale that explains the selectivity of the inhibitor towards the delta isoform is provided. A change in the C-terminal residues would be expected to disrupt the interactions identified to stabilise the roginolisib-induced kα12 conformation. Furthermore, the p85α cSH2 domain does not inhibit p110α [15] and also the p101 regulatory subunit has no interactions with the C-terminus of the γ isoform [31]. Given the absence of Lys1040 and Arg1043 in the α and γ isoforms and the lack of the cSH2 type inhibition, roginolisib is predicted to be selective for p110δ, and to a lesser extent for the β isoform. This is consistent with in vitro IC50 measurements [19], demonstrating over 500- and 1,000-fold selectivity against the α and γ isoforms, respectively, with comparatively low selectivity against the β isoform (Fig. S7b).

Idelalisib and roginolisib have a limited effect on PI3Kδ affinity for membrane binding upon stimulation

HDX-MS analysis has shown that the kα1-kα2 loop conformation is altered upon binding of either roginolisib or idelalisib in solution, raising the question of whether inhibitor binding could modulate membrane interaction. To understand if the presence of inhibitors affects PI3Kδ membrane interaction, we examined the binding of PI3Kδ to lipid membranes in presence of idelalisib and roginolisib using protein-lipid FRET assays [15]. To phosphorylate their substrate, PI3Ks must be at the membrane and affinity with membranes is mostly controlled by the regulatory p85 subunit for class IA PI3Ks. The p110 catalytic subunit makes direct contacts with the membrane involving the C-terminal catalytic domain. In the inhibited state, access to membrane of the p110δ subunit is blocked by the interaction of the cSH2 domain of p85α with the hinge between helices kα11 and kα12. Engagement of the cSH2 with phosphorylated tyrosines present on the cytosolic side of RTKs both disrupts the inhibitory contact with

the p110δ catalytic subunit and positions the enzyme in proximity to the plasma membrane. As non-stimulated PI3Kδ has only a low affinity for membranes, we measured binding affinities in presence of an excess of a phosphopeptide (pY PDGFR), mimicking receptor tyrosine kinase engagement at the membrane. When testing on vesicles mimicking plasma membrane composition, stimulation with pY showed a 4-fold increase in membrane affinity, with an approximately 20% decrease upon inhibitor binding (supplementary Fig. S8). This shows that the change in conformations of membrane-interacting kα1-kα2 and kα12 helixes have only a limited effect on lipid interactions, at least for the pY-stimulated PI3Kδ heterodimer.

The insertion of kα12 in the membrane primes p110δ for catalysis

The kα12 helix of PI3Ks has previously been implicated in membrane binding (Fig. S9) [15,30,31,34]. To further examine its role in the membrane targeting of PI3Kδ, we performed MD simulations of ATP-bound p110δ in the presence of PI(4,5)P2-containing membranes with a lipid composition approximating that of the leukocytic plasma membrane [35]. Initially with its active site oriented towards the membrane and at a distance of 2 nm from the nearest lipid (Fig. 6a), p110δ formed spontaneous membrane association, with over 60 protein residues brought into contact with membrane lipids in the first 500 ns of one simulation replicate (Fig. 6b and c). The first contacts were made by a loop region between β-sheet strands β5 and β6 of the C2 domain. The nine basic residues on the C2 β5/β6 loop established persistent interactions with negatively charged lipid headgroups (Fig. 6b) within ~ 50 ns of simulation time. Subsequent membrane contacts of the C-terminal kα12 helix, initiated by its Lys1028 interacting with PIP2, led to spontaneous insertion of kα12 into the membrane. The helix remained stably embedded in between lipid acyl chains through the duration of the 3 μs simulation (Fig. 6b and c). Its C-terminal end became more ordered in the membrane-bound state, which is consistent with the finding that in the class II PI3KC2α kα12 tends to be more structured in the active than in the inactive state [32]. Membrane insertion of kα12 was accompanied by formation of extensive protein-membrane interactions, and the interaction interface was maintained over the simulation timescale (Fig. 7). The stable interface of membrane contacts, formed by the N- and C-lobe, are in agreement with regions previously identified by HDX measurements [15]. The C2 domain membrane contacts were not observed by HDX which may suggest that these interactions are less likely in presence of p85.

Notably, we observed spontaneous binding of a molecule of the lipid substrate, PIP2, into the kinase active site (Fig. 8). The PIP2 inositol ring interacted in close proximity with the γ-phosphate of the bound ATP, suggesting a configuration compatible with catalysis of the phosphate transfer reaction. Analyses of protein contacts stabilising the bound PIP2 revealed persistent interactions with Arg1043 and, to a lesser extent, Lys1040. We therefore repeated the simulations (5 replicates) with kα12 deleted. While p110δ remained membrane bound in these simulations, likely mediated by interaction of the C2 domain, the substrate PIP2 dissociated from the active site. This may explain the earlier finding that truncation of kα12 drastically reduces lipid kinase activity [28].

Roginolisib leads to an efficient PIP3 decrease in double–refractory CLL patient cells

The activity of roginolisib on CLL patient samples as measured by the suppression distal markers such as phosphorylation of AKT, ERK, FOXO1 and GSK3α/β has been reported to be comparable to that seen with idelalisib or duvelisib [36]. To investigate whether the differences in binding modes translate into changes in actual kinase activity, we utilized a mass spectrometry–based approach to quantify PIP3 in cell lysates from CLL patient samples treated ex vivo with roginolisib and idelalisib at two fixed doses and time points. Samples were obtained from both treatment naïve patients and patients refractory to BTK- and BCL-2 inhibitors. The analysis revealed that roginolisib was more effective in decreasing PIP3 levels, especially at the 2-hour time point (Fig. 9). It was equally efficient in all the patients tested. Idelalisib on the other hand led to a heterogeneous response between patients, with one naïve and two double refractory patients presenting an increased peak of PIP3 production compared to vehicle and roginolisib at either 2h or 24h, indicative of treatment resistance (Fig. 9). These findings may suggest that stabilization of the inhibited form of PI3Kδ leads to more robust suppression of the kinase activity compared to ATP competitive inhibition of the active kinase at the plasma membrane.

Discussion

Designing selective ATP-competitive lipid kinase inhibitors is a challenge based on the conserved ATP-binding pocket. Improved inhibitor selectivity can be achieved by exploiting binding sites and regulatory features that are unique to individual kinases [37,38]. Kinases continuously cycle between productive (active) and non-productive (inactive) states and since the inactive state potentially can adopt a distinct conformation, targeting the inactive state of a kinase is an attractive strategy to discover selective inhibitors. The latter may also not compete with ATP for binding [39]. In protein kinases this approach is widely used as exemplified by the so-called type II and type III inhibitors, which induce a distinct DFG-out conformation and bind in an additional hydrophobic pocket created by this rearrangement, or bind to an allosteric pocket adjacent or remote to the ATP- binding site, respectively [40,41]. Lipid kinase inhibitor design is less advanced and the first allosteric isoform-mutant selective PI3K inhibitors have only recently entered clinical trials [4]. In parallel with efforts to identify inhibitors, a PI3Kα-selective allosteric activator was recently described, which provides cardioprotection from ischaemia-reperfusion injury [42]. This activator enhances multiple steps of the PI3Kα catalytic cycle, highlighting the benefit of studying enzyme regulation to design selective drugs with non-conventional modes of action.

Despite the availability of several crystal structures, little is known about which activation states are targeted by the different PI3K inhibitors. In class I PI3Ks, a key regulatory element is the regulatory arch composed of the C-terminal helices kα10-kα11-kα12, which encircles the catalytic- and activation loops essential for kinase activity [16]. Activation of all class I PI3Ks requires a reorientation of the C-terminus of the kinase domain to bind to lipid membranes where they are further activated by Ras to exert their function. For full activation, the regulatory arch needs to open, allowing the catalytic site to be in close proximity to the membrane bound lipid substrate [15].

The C-terminal helix kα12 has been reported to have a crucial role in PI3K catalysis. It was initially studied in the class III PI3K, Vps34, where the equivalent region was shown to be auto-inhibitory in the absence of lipid substrate but would bind to the cell membrane and facilitate kinase activity [30,43]. Based on HDX-MS experiments and kinase activity measurements, a similar mechanism of membrane binding and activation has since been suggested for the class I PI3Ks [15,28,31]. Truncation of kα12 completely removes all lipid kinase activity [28]. The importance of kα12 for catalysis is further highlighted by the gain or loss of PI3K function associated with mutations in the C-terminal region [44]. Autophosphorylation of p110δ Ser1039 was also shown to downregulate PI3Kδ lipid kinase activity [45]. In available co-crystal structures of the β and γ PI3K isoforms [28,34,46], the C-terminus adopts a bent conformation with a hinge between the C-terminal helices kα11 and kα12. The conformation where the C-terminal helix kα12 covers the catalytic as well as the activation loop is considered the inactive state of the kinase [28,47]. A similar C-terminal helix configuration has been predicted by AlphaFold [27] for PI3Kδ, in which the ~18 C-terminal residues have been unresolved in experimental co-crystal structures of the protein.

We have used X-ray co-crystal structure data, molecular dynamics simulations, HDX-MS studies and PIP3 formation in CLL patient samples to shed light on the mode of action of the next generation PI3Kδ-selective inhibitor roginolisib. Notably, major differences with the clinically approved first generation PI3Kδ inhibitor idelalisib were identified that may contribute to the improved tolerability of roginolisib in patients [Di Giacomo et al co-submitted]. We found that roginolisib binding to PI3Kδ shows several differences compared to idelalisib. Roginolisib does not occupy the specificity pocket in PI3Kδ and the orientation of the side chains of Asp911 of the DFG motif and Asp897 are altered compared to idelalisib. Although these differences demonstrate a differentiated binding mode of roginolisib, they do not explain its selectivity nor its potency in the presence of high ATP concentrations. Because of the absence of electronic density for the catalytically important kα12 helix in the PI3Kδ crystal structures, we turned to MD simulations and HDX-MS experiments to investigate how these changes may affect its conformation.

MD simulations on the full-length p110δ Alphafold model in complex with roginolisib showed that the two acidic residues Asp911 and Asp897 can interact with Lys1040 and Arg1043 of helix kα12, forming an electrostatic stabilisation contact. This results in a stabilization of the C-terminus in a bent conformation with the kα12 helix in a position that covers the active site, likely indicative of the PI3Kδ inactive state. The observed unfolding of the C-terminal half of kα12 provides the required flexibility for these interactions to occur in a similar manner to the reported stabilisation of the inactive conformation of PI3KC2α [32]. In contrast, such conformational stabilization of kα12 was not seen for the MD simulations done for the p110δ-idelalisib complex, which favoured an opened regulatory arch that is more in accordance with a partially activated state [14]. The fact that ATP binding requires interaction of Lys1040 and Arg1043 with the gamma-phosphate of ATP, likely attenuates the ATP affinity for roginolisib bound PI3Kδ. Occupation of the ATP-binding pocket combined with the electrostatic stabilisation of residues critical for nucleotide binding may thus explain why roginolisib maintains its potency at high

ATP concentration [19]. The residues Lys1040 and Arg1043 are unique to the δ and β isoforms and therefore also explain the selectivity of roginolisib for p110δ, and to a lesser extent for the β isoform.

The stabilisation of helix kα12 by roginolisib was confirmed experimentally by HDX-MS. Comparison of the PI3Kδ H/D exchange profiles in absence and presence of either roginolisib or idelalisib showed that binding of each ligand has minimal impact on the global enzyme conformation. The hinge region of p110δ was protected by both molecules, as expected for inhibitors binding to the ATP-pocket. Both ligands also triggered conformational rearrangements in helices kα1-kα2 of the kinase domain, a region previously shown to mediate interactions with the p85α-cSH2 domain and membranes [15]. This change has limited impact on the membrane affinity of phosphopeptide-stimulated PI3Kδ, further supporting the inhibitors mechanism of action affecting primarily the enzyme's catalytic function. Protection from H/D exchange of helix kα12 was only seen when in complex with roginolisib. This protection indicates a stabilisation of the helix, owing to direct contacts with active site residues. It also supports a potential positioning of the helix in a bent inward-facing orientation, thus blocking the access to the active site. The observed protection of the helix kα12 is lost upon removal of the p85α-cSH2 inhibitory interaction in the p85α-Y685A mutant. These findings combined with the absence of exposure of the kα11-kα12 elbow region upon roginolisib binding support a mechanism where the binding of the cSH2 domain of p85α to p110δ is important for stabilizing the roginolisib bound complex. Since the PI3Kα and -γ lack the autoinhibitory cSH2 interaction, this mechanism further supports the high selectivity of roginolisib over these isoforms.

To further explore the conformation changes of kα12 upon membrane binding, MD simulations of ATP-bound p110δ in the presence of PIP2-containing membranes were performed. These simulations confirmed that kα12 readily and stably inserts into the membrane, likely facilitated by the observed increased ordering of the helix structure. Furthermore, spontaneous binding of PIP2 in the active site was observed. Interestingly PIP2 binding was stabilised through interactions with Arg1043 and Lys1040, the same residues involved in stabilising the roginolisb bound inactive kinase conformation. Removal of kα12 resulted in dissociation of PIP2 from the active site.

The combined MD simulations and HDX-MS experiments point toward roginolisib having a conformation-selective inhibitory mechanism, targeting specifically the inhibited enzyme and thereby hindering binding of both ATP and PIP2. Idelalisib on the other hand does not discriminate between active and inactive states since no bending of the C-terminal region was observed by MD simulations with idelalisib and its H/D exchange profiles remained similar for WT and activated PI3Kδ. The more robust inhibition of PIP3 formation in ex vivo treated CLL patient samples observed for roginolisib compared to idelalisib may further suggest that selective targeting of the inhibited enzyme is more efficacious for attenuating pathological PI3Kδ signalling. Furthermore, roginolisib is highly efficient to decrease PIP3 levels in double-refractory patients, patients resistant to the current treatment, consisting of first line ibrutinib, and second line of ibrutinib plus veneteoclax treatment. Idelalisib does not work as well in double refractory patients compared to naïve patients. Increased accumulation of PIP3 has also been observed in post-idelalisib therapy CLL cells from patients and was explained by increased

recruitment of PI3Kδ and/or PI3Kβ to the B cell receptor (BCR) complex [48]. Whether roginolisib binding affects this recruitment is a topic of current investigation.

In summary, high selectivity is a prerequisite for designing safe PI3K inhibitors. The first generation of PI3Kδ inhibitors aimed to achieve selectivity and potency towards p110δ by exploiting conformational flexibility of the enzyme in the ATP-binding pocket and inducing the formation of the specificity pocket [21]. Our work shows that roginolisib, binding in the ATP pocket but not interacting with the specificity pocket, inhibits the enzyme by stabilizing an inactive conformation. This is achieved by locking the p110δ-kα12 helix in an inactive conformation. To our knowledge, this is the first time that the protein dynamic effects of inhibitor binding on PI3Kδ have been investigated. This work demonstrates that roginolisib is a conformation-selective inhibitor and this inhibition mode for PI3Kδ not only results in high isoform selectivity and improved efficacy but also contributes to an improved safety profile in cancer patients. Ongoing studies aim to determine whether this stabilization leads to further distinct biological effects.

Methods

Protein crystallography

The complex of human p110δ (amino acids 1-1044 preceded by an N-terminal cleavable HIS-tag) and bovine p85 (amino acids 431–600, no tag) was co-expressed in Sf9 cells at 26°C from two separate viruses. Cells were harvested 48 hours after infection and the p110δ/p85 complex was purified by a three-step chromatographic procedure at 4°C. Briefly, the pellet from a 5L expression culture was lysed using an Ultra-Turrax and the lysate was centrifuged for 30 minutes at 75,000 × g. Protein was captured in batch mode by adding 12mL of Ni Sepharose HP beads to the supernatant and incubating the suspension for 2h. Beads were poured in an XK16/20 column and bound protein was recovered by imidazole elution. The HIS-tag was removed by overnight incubation with TEV-protease and protein was passed over the Ni-column used for the initial capture step. Protein complex in the flow-through was collected and purified to homogeneity on a Superdex200 26/60 column equilibrated in 50mM Tris/HCl, 150mM NaCl and 1.5mM DTT. For crystallization, protein at 5 mg/mL concentration was incubated with the compound and crystallized by vapor diffusion in hanging drops. Equal volumes (1μL:1μL) of protein and reservoir solution (12–14% PEG 6000, 100mM MES/NaOH at pH = 5.75) were mixed and equilibrated against 1mL of reservoir solution containing 5mM DTT at 20°C. Protein crystals that grew within 2–3 days were optimized for diffraction by using the Free Mounting System™ [49] and frozen for data collection.

Molecular dynamics simulations

Initial structures of full-length p110δ in complex with either idelalisib (PDB ID: 4XE0 [50]) or roginolisib were modelled using MODELLER [51] based on the best-ranked p110δ Alphafold model [27] and structures of the respective protein-ligand X-ray co-crystals. The ATP-bound structure is based on a crystal

structure of the ATP-bound p110γ isoform (PDB ID: 1E8X [34]) with the relative position of the coordinated magnesium ion from PDB ID: 1CSN [52]. The co-crystallised p85 iSH2 domain in the roginolisib-bound structure was included in two simulations of the complex in solution and removed in all other simulations. MD simulations were performed in Gromacs 2020 [53], using the AMBER99SB*-ILDN-q force field [54–57] and CHARMM36m [58] force fields, respectively, for simulations of the protein-ligand complex in solution and in the presence of membranes.

For simulations of the kinase domain in solution, the protein-ligand complexes were solvated with TIP3P water[59] and 150 mM NaCl. The resulting dodecahedron simulation boxes were of size ~2200 nm^3 and contained ~215,000 atoms. Particle-mesh Ewald electrostatics were used [60]. Upon energy minimization, five stages of equilibration were performed, in which the positional restraints on protein heavy atoms were successively decreased, first in an NVT ensemble (0.25 ns) and subsequently in an NPT ensemble (4 × 0.5 ns) using a Berendsen thermostat and barostat [61]. Production runs were performed in NPT, with an integration time step of 2 fs. Five replicates were prepared per system. The duration of simulation replicates were 500 ns in the case of ATP-bound p110δ and between 2 μs (four out of five replicates) and 5 μs (one replicate) for the roginolisib- or idelalisib-bound protein. Temperature was maintained at 310 K using a Nosé-Hoover thermostat [62,63], with the pressure maintained at 1 bar using an isotropic Parrinello-Rahman barostat [64].

For protein-membrane simulations, the membrane lipid composition was based on a leucocytic plasma membrane lipid composition [35] consisting of 15% dioleoylphosphatidylcholine (DOPC), 10% 1-palmitoyl-2-oleoyl-sn-glycero-3-phosphocholine (POPC), 15% dioleoylphosphatidyl-ethanolamine (DOPE), 15% 1-palmitoyl-2-oleoyl-sn-glycero-3-phosphoethanolamine (POPE), 35% cholesterol, 5% 1-palmitoyl-2-oleoyl-sn-glycero-3-phosphoserine (POPS), and 5% PIP2 for both leaflets. Membranes were constructed initially in a coarse-grained representation using the insane method [65]. Six independent replicates were prepared, each with a random distribution of lipid species and solvated with 150 mM of aqueous NaCl. Coarse-grained membrane systems were equilibrated for 200 ns and converted into atomistic representation using the CG2AT2 tool [66]. The ATP-bound p110δ structure was placed above each upper membrane leaflet with a minimum distance of 2 nm between protein and lipid atoms, and the height of the simulation box was increased to 20 nm. The final protein-membrane systems, containing ~ 350,000 atoms, were re-solvated with 150 mM of NaCl using TIP3P water [59] and further equilibrated for 10 ns prior to 2 μs production simulations. The simulation replicate in which membrane insertion of kα12 occurred was subsequently extended to a total duration of 3 μs. Harmonic positional restraints were applied to non-hydrogen protein atoms during equilibration, with a force constant of 1000 kJ mol-1 nm-2. System temperature and pressure were maintained at 310 K and 1 bar, using the velocity-rescaling thermostat [67] and a semi-isotropic Parrinello-Rahman barostat [64] in the production phase. The integration time step was 2 fs. Long-range electrostatic interactions were treated using the smooth particle mesh Ewald method [60,68]. The LINCS algorithm was used to constrain covalent bonds involving hydrogen atoms [69]. Simulation trajectories were analysed through MDAnalysis 2.0 [70] in Python 3.6.

Lipid vesicle preparation for membrane affinity assays

Dansyl-containing lipid vesicles mimicking plasma membrane composition were prepared with the following composition: 5% Brain PI(4,5)P2; 10% Dansyl PS; 20% Brain PS, 35% DOPE; 15% DOPC; 10% Cholesterol; 5% Sphingomyelin. Lipids were mixed in organic solvent before evaporation with nitrogen flow and dessication under vacuum for 15 h at 22°C. Lipids were resuspended in lipid buffer (20 mM Hepes pH 7.5, 100mM KCl, 1 mM EGTA) at a concentration of 1 mg/ml. Vesicles were sonicated for 10 min, subjected to five freeze-thaw cycles and extruded 17 times through a 100 nm filter. Aliquots were flash-frozen in liquid nitrogen and stored at -80°C.

Protein-lipid FRET assays

Protein-lipid FRET assays were performed in 384-well plates at different PI3Kδ concentrations while keeping phosphopeptide, lipids and inhibitors at a fixed concentration. Serial dilutions of PI3Kδ were made in a final 9 µl volume in assay buffer (20 mM Tris pH 7.4, 150 mM NaCl, 2 mM DTT) supplemented with either 10 µM PDGFR pY peptide (pY) and/or 20 µM inhibitor. Concentrations of PI3Kδ ranging from 3000 nM to 44 nM were prepared by performing 1.7-fold dilution in assay buffer supplemented with the defined peptide and/ or pY. Following 15 min incubation at 22°C, 9 µl of lipid solution at 200 µg/ml was added and the reaction mixed was incubated for another 15 min at 22°C. The plate was then read using a BMG Labtech plate reader using 280 nm excitation filter with 350 nm and 520 nm emission filters to measure tryptophan and Dansyl PS FRET emisissions respectively. The FRET signal shown in Fig S8 has I-Io along the Y axis where I is the intensity of 520 with protein and Io is the intensity of lipid alone.

PIP extraction from patient samples and measurement by mass spectrometry

Peripheral blood samples from untreated (n = 3) and double refractory (n = 3) CLL patients were obtained from the Hematology Department of the IUCT-Oncopole, Toulouse, France, with informed consent and referenced in the Inserm cell bank. To allow storage of ibrutinib and venetoclax treated patient cells, studies were approved by the competent authority (ANSM, n° 1551668A-11), the ethics committee (N° CPP16-004a) and registered with Clinical-Trials.gov (NCT02824159 and NCT02005471). For storage and use of all patient samples, Inserm cell bank has been registered with the Ministry of Higher Education and Research (DC- 2013 – 1903) after being approved by an ethic committee. Clinical and Biological annotations of the samples have been reported to the Comité National Informatique et Liberté.

PBMCs from CLL patients were seeded at 5×10^6 cells/ml in culture medium (providing long-term viability). Circulating tumor cells from patients were treated with or without the vehicle (DMSO) or Idelalisib or roginolisib (0.5 µM) for 2 or 24 hours. The cells were collected and centrifuged at 800 g at 4°C for 5 min; the culture medium was quickly aspirated and cells were resuspended in cold HCl 1M. The lysate was centrifuged for 5 minutes at 15,000 g at 4°C. The cell pellet was stored at -80°C until required for PIP extraction. Lipids were extracted and derivatised using TMS-diazo-methane as described by Clark et al [71]. Mass spectral analysis was performed on the LC-QqQ triple quadrupole mass spectrometer (LC-vcQQQ 6460 Agilent) equipped with positive mode electrospray ionisation as described by Thibault et al

[72]. Analyses were performed in Selected Reaction Monitoring detection mode (SRM) using nitrogen as collision gas. Finally, peak detection, integration and quantitative analysis were performed using MassHunter QqQ Quantitative analysis software (Agilent Technologies VersionB.05.00) and Microsoft Excel software. Data were processed using QqQ Quantitative (vB.05.00) and Qualitative analysis software (vB.04.00).

Declarations

Data Availability

Source data are provided with this paper in the supplementary material, including for the HDX-MS experiments (Tables S3, S4 and S5). The X-ray structures have been submitted to the protein data bank (PDB) under IDs 9T07 (roginolisib) and 9T1P (IOA-288). Any other relevant data, including the MD simulations, are available from the corresponding authors upon reasonable request.

Contributions

Each author has approved the submitted version (and any substantially modified version) of this manuscript. O.V. contributed to HDX-MS experiments and analysis, and manuscript drafting. S.T., L.T., S.R. and G.H. each contributed to MD simulations and analysis, and manuscript drafting or revision. M.C and J.G.G. contributed to CLL patient sample experiments, and manuscript drafting or revision. R.V. contributed to HDX-MS experiments and analysis. U.G. contributed to crystal structure analysis and manuscript drafting. M.A., R.K. and C.G. contributed to solving the crystal structures. A.Q.M. and L.Y. contributed to CLL patient sample experiments. L.V.V and G.D.C. contributed to manuscript drafting and revision.

Acknowledgements (optional)

The authors would like to thank Alexandre Hainard from the proteomics platform at the University of Geneva for assistance in HDX-MS data acquisition. Justine Bertrand-Michel for the lipidomics platform (MetaToul-Lipidomique Core Facility, I2MC, Inserm 1048, Toulouse, France) and the IUCT clinicians and patients who provided samples. The project on CLL cells has received funding from the European Union's Horizon 2020 research and innovation programme under the Marie Skłodowska-Curie grant agreement No 955534. This research was further supported by the Max Planck Society, and the authors thank the Max Planck Computing and Data Facility for computational support. Medical writing support was provided by Dr Gareth Hardy of Niche Science and Technology Ltd, Richmond-Upon-Thames, London, UK

Ethics declarations

Competing interests

L.V.V and G.D.C. are employees of the study Sponsor (iOnctura).

Supplementary Information

Supplementary Information is combined and supplied as a separate file.

References

1. Vanhaesebroeck, B., Perry, M. W. D., Brown, J. R., André, F. & Okkenhaug, K. PI3K inhibitors are finally coming of age. *Nat Rev Drug Discov* 1–29 (2021) doi:10.1038/s41573-021-00209-1.
2. Bilanges, B., Posor, Y. & Vanhaesebroeck, B. PI3K isoforms in cell signalling and vesicle trafficking. *Nat Rev Mol Cell Bio* **20**, 515–534 (2019).
3. Yap, T. A., Bjerke, L., Clarke, P. A. & Workman, P. Drugging PI3K in cancer: refining targets and therapeutic strategies. *Curr Opin Pharmacol* **23**, 98–107 (2015).
4. Cirillo, D., Diceglie, M. & Nazaré, M. Isoform-selective targeting of PI3K: time to consider new opportunities? *Trends Pharmacol. Sci.* **44**, 601–621 (2023).
5. Vanhaesebroeck, B. *et al.* p110 , a novel phosphoinositide 3-kinase in leukocytes. *Proc National Acad Sci* **94**, 4330–4335 (1997).
6. Chantry, D. *et al.* p110δ, a Novel Phosphatidylinositol 3-Kinase Catalytic Subunit That Associates with p85 and Is Expressed Predominantly in Leukocytes*. *J. Biol. Chem.* **272**, 19236–19241 (1997).
7. Okkenhaug, K. & Vanhaesebroeck, B. PI3K in lymphocyte development, differentiation and activation. *Nat Rev Immunol* **3**, 317–330 (2003).
8. Meng, D. *et al.* Development of PI3K inhibitors: Advances in clinical trials and new strategies (Review). *Pharmacol. Res.* **173**, 105900 (2021).
9. Yang, Q., Modi, P., Ramanathan, S., Quéva, C. & Gandhi, V. Idelalisib for the treatment of B-cell malignancies. *Expert Opin Orphan D* **3**, 109–123 (2014).
10. Richardson, N. C., Kasamon, Y., Pazdur, R. & Gormley, N. The saga of PI3K inhibitors in haematological malignancies: survival is the ultimate safety endpoint. *Lancet Oncol* (2022) doi:10.1016/s1470-2045(22)00200-5.
11. Gadkar, K. *et al.* Quantitative systems pharmacology model-based investigation of Adverse Gastrointestinal Events Associated with Prolonged Treatment with PI3-Kinase (PI3K) Inhibitors. *Cpt Pharmacometrics Syst Pharmacol* (2021) doi:10.1002/psp4.12749.
12. Veen, L. van der, Schmitt, M., Deken, M. A. & Lahn, M. Non-Clinical Toxicology Evaluation of the Novel Non-ATP Competitive Oral PI3 Kinase Delta Inhibitor Roginolisib. *Int. J. Toxicol.* 10915818231200419 (2023) doi:10.1177/10915818231200419.
13. Buckbinder, L. *et al.* STX-478, a Mutant-Selective, Allosteric PI3Ka Inhibitor Spares Metabolic Dysfunction and Improves Therapeutic Response in PI3Ka-Mutant Xenografts. *Cancer Discov.* **13**, 2432–2447 (2023).
14. Vadas, O., Burke, J. E., Zhang, X., Berndt, A. & Williams, R. L. Structural Basis for Activation and Inhibition of Class I Phosphoinositide 3-Kinases. *Sci. Signal.* **4**, re2 (2011).

15. Burke, J. E. *et al.* Dynamics of the Phosphoinositide 3-Kinase p110δ Interaction with p85α and Membranes Reveals Aspects of Regulation Distinct from p110α. *Struct Lond Engl 1993* **19**, 1127–1137 (2011).
16. Burke, J. E. Structural Basis for Regulation of Phosphoinositide Kinases and Their Involvement in Human Disease. *Mol Cell* **71**, 653–673 (2018).
17. Siempelkamp, B. D., Rathinaswamy, M. K., Jenkins, M. L. & Burke, J. E. Molecular mechanism of activation of class IA phosphoinositide 3-kinases (PI3Ks) by membrane-localized HRas. *J Biol Chem* **292**, 12256–12266 (2017).
18. Giacomo, A. M. D. *et al.* Safety and Clinical Benefit Assessment of Continuous Roginolisib Administration in Patients with Cancer including Metastatic Uveal Melanoma. *Nature Comms, submitted*.
19. Johnson, Z. *et al.* IOA-244 is a non-ATP-competitive, highly selective, tolerable phosphoinositide 3-kinase delta inhibitor that targets solid tumors and breaks immune tolerance. *Cancer Res Commun* (2023) doi:10.1158/2767-9764.crc-22-0477.
20. Kuhn, B., Fuchs, J. E., Reutlinger, M., Stahl, M. & Taylor, N. R. Rationalizing Tight Ligand Binding through Cooperative Interaction Networks. *J. Chem. Inf. Model.* **51**, 3180–3198 (2011).
21. Berndt, A. *et al.* The p110δ structure: mechanisms for selectivity and potency of new PI(3)K inhibitors. *Nat Chem Biol* **6**, 117 (2010).
22. Hubbard, S. R., Wei, L., Ellis, L. & Hendrickson, W. A. Crystal structure of the tyrosine kinase domain of the human insulin receptor. *Nature* **372**, 746–754 (1994).
23. Hubbard, S. R. Crystal structure of the activated insulin receptor tyrosine kinase in complex with peptide substrate and ATP analog. *EMBO J.* **16**, 5572–5581 (1997).
24. Peng, Y.-H. *et al.* Protein Kinase Inhibitor Design by Targeting the Asp-Phe-Gly (DFG) Motif: The Role of the DFG Motif in the Design of Epidermal Growth Factor Receptor Inhibitors. *J. Med. Chem.* **56**, 3889–3903 (2013).
25. Zuccotto, F., Ardini, E., Casale, E. & Angiolini, M. Through the "Gatekeeper Door": Exploiting the Active Kinase Conformation. *J. Med. Chem.* **53**, 2681–2694 (2010).
26. Ung, P. M.-U. & Schlessinger, A. DFGmodel: Predicting Protein Kinase Structures in Inactive States for Structure-Based Discovery of Type-II Inhibitors. *ACS Chem. Biol.* **10**, 269–278 (2015).
27. Jumper, J. *et al.* Highly accurate protein structure prediction with AlphaFold. *Nature* **596**, 583–589 (2021).
28. Zhang, X. *et al.* Structure of Lipid Kinase p110β/p85β Elucidates an Unusual SH2-Domain-Mediated Inhibitory Mechanism. *Mol Cell* **41**, 567–578 (2011).
29. Walker, E. H., Perisic, O., Ried, C., Stephens, L. & Williams, R. L. Structural insights into phosphoinositide 3-kinase catalysis and signalling. *Nature* **402**, 313–320 (1999).
30. Miller, S. *et al.* Shaping Development of Autophagy Inhibitors with the Structure of the Lipid Kinase Vps34. *Science* **327**, 1638–1642 (2010).

31. Vadas, O. *et al.* Molecular determinants of PI3Kγ-mediated activation downstream of G-protein–coupled receptors (GPCRs). *Proc. Natl. Acad. Sci.* **110**, 18862–18867 (2013).
32. Lo, W.-T. *et al.* Structural basis of phosphatidylinositol 3-kinase C2α function. *Nat Struct Mol Biol* **29**, 218–228 (2022).
33. Stariha, J. T. B., Hoffmann, R. M., Hamelin, D. J. & Burke, J. E. Protein-Ligand Interactions, Methods and Applications. *Methods Mol. Biol.* **2263**, 465–485 (2021).
34. Walker, E. H. *et al.* Structural Determinants of Phosphoinositide 3-Kinase Inhibition by Wortmannin, LY294002, Quercetin, Myricetin, and Staurosporine. *Mol. Cell* **6**, 909–919 (2000).
35. GOTTFRIED, E. L. Lipid patterns in human leukocytes maintained in long-term culture. *J. Lipid Res.* **12**, 531–537 (1971).
36. Sasi, B. K. *et al.* Novel Pi3kδ Inhibitor Roginolisib Synergizes with the Bcl-2 Inhibitor Venetoclax in Hematological Malignancies. *Blood* **142**, 4179 (2023).
37. Knight, Z. A. & Shokat, K. M. Features of Selective Kinase Inhibitors. *Chem Biol* **12**, 621–637 (2005).
38. Kirkland, L. O. & McInnes, C. Non-ATP competitive protein kinase inhibitors as anti-tumor therapeutics. *Biochem Pharmacol* **77**, 1561–1571 (2009).
39. Eathiraj, S. *et al.* A Novel Mode of Protein Kinase Inhibition Exploiting Hydrophobic Motifs of Autoinhibited Kinases DISCOVERY OF ATP-INDEPENDENT INHIBITORS OF FIBROBLAST GROWTH FACTOR RECEPTOR. *J Biol Chem* **286**, 20677–20687 (2011).
40. Garuti, L., Roberti, M. & Bottegoni, G. Non-ATP Competitive Protein Kinase Inhibitors. *Curr Med Chem* **17**, 2804–2821 (2010).
41. Fabbro, D. 25 Years of Small Molecular Weight Kinase Inhibitors: Potentials and Limitations. *Mol Pharmacol* **87**, 766–775 (2015).
42. Gong, G. Q. *et al.* A small-molecule PI3Kα activator for cardioprotection and neuroregeneration. *Nature* **618**, 159–168 (2023).
43. Budovskaya, Y. V., Hama, H., DeWald, D. B. & Herman, P. K. The C Terminus of the Vps34p Phosphoinositide 3-Kinase Is Necessary and Sufficient for the Interaction with the Vps15p Protein Kinase*. *J. Biol. Chem.* **277**, 287–294 (2002).
44. Rathinaswamy, M. K. *et al.* Disease-related mutations in PI3Kγ disrupt regulatory C-terminal dynamics and reveal a path to selective inhibitors. *Elife* **10**, e64691 (2021).
45. Vanhaesebroeck, B. *et al.* Autophosphorylation of p110δ phosphoinositide 3-kinase: a new paradigm for the regulation of lipid kinases in vitro and in vivo. *Embo J* **18**, 1292–1302 (1999).
46. Certal, V. *et al.* Discovery and Optimization of Pyrimidone Indoline Amide PI3Kβ Inhibitors for the Treatment of Phosphatase and Tensin Homologue (PTEN)-Deficient Cancers. *J. Med. Chem.* **57**, 903–920 (2014).
47. Gangadhara, G. *et al.* A class of highly selective inhibitors bind to an active state of PI3Kγ. *Nat Chem Biol* **15**, 348–357 (2019).

48. Mamidi, M. K. *et al.* Idelalisib activates AKT via increased recruitment of PI3Kδ/PI3Kβ to BCR signalosome while reducing PDK1 in post-therapy CLL cells. *Leukemia* **36**, 1806–1817 (2022).
49. Kiefersauer, R. *et al.* A novel free-mounting system for protein crystals: transformation and improvement of diffraction power by accurately controlled humidity changes. *J. Appl. Crystallogr.* **33**, 1223–1230 (2000).
50. Somoza, J. R. *et al.* Structural, Biochemical, and Biophysical Characterization of Idelalisib Binding to Phosphoinositide 3-Kinase δ*. *J Biol Chem* **290**, 8439–8446 (2015).
51. Šali, A. & Blundell, T. L. Comparative Protein Modelling by Satisfaction of Spatial Restraints. *J. Mol. Biol.* **234**, 779–815 (1993).
52. Xu, R. M., Carmel, G., Sweet, R. M., Kuret, J. & Cheng, X. Crystal structure of casein kinase-1, a phosphate-directed protein kinase. *EMBO J.* **14**, 1015–1023 (1995).
53. Abraham, M. J. *et al.* GROMACS: High performance molecular simulations through multi-level parallelism from laptops to supercomputers. *SoftwareX* **1**, 19–25 (2015).
54. Meagher, K. L., Redman, L. T. & Carlson, H. A. Development of polyphosphate parameters for use with the AMBER force field. *J. Comput. Chem.* **24**, 1016–1025 (2003).
55. Hornak, V. *et al.* Comparison of multiple Amber force fields and development of improved protein backbone parameters. *Proteins: Struct., Funct., Bioinform.* **65**, 712–725 (2006).
56. Best, R. B. & Hummer, G. Optimized Molecular Dynamics Force Fields Applied to the Helix−Coil Transition of Polypeptides. *J. Phys. Chem. B* **113**, 9004–9015 (2009).
57. Lindorff-Larsen, K. *et al.* Improved side-chain torsion potentials for the Amber ff99SB protein force field. *Proteins: Struct., Funct., Bioinform.* **78**, 1950–1958 (2010).
58. Huang, J. *et al.* CHARMM36m: an improved force field for folded and intrinsically disordered proteins. *Nat. Methods* **14**, 71–73 (2017).
59. Jorgensen, W. L., Chandrasekhar, J., Madura, J. D., Impey, R. W. & Klein, M. L. Comparison of simple potential functions for simulating liquid water. *J. Chem. Phys.* **79**, 926–935 (1983).
60. Darden, T., York, D. & Pedersen, L. Particle mesh Ewald: An N ·log(N) method for Ewald sums in large systems. *J. Chem. Phys.* **98**, 10089–10092 (1993).
61. Berendsen, H. J. C., Postma, J. P. M., Gunsteren, W. F. van, DiNola, A. & Haak, J. R. Molecular dynamics with coupling to an external bath. *J. Chem. Phys.* **81**, 3684–3690 (1984).
62. Nosé, S. A unified formulation of the constant temperature molecular dynamics methods. *J. Chem. Phys.* **81**, 511–519 (1984).
63. Hoover, W. G. Canonical dynamics: Equilibrium phase-space distributions. *Phys. Rev. A* **31**, 1695–1697 (1985).
64. Parrinello, M. & Rahman, A. Polymorphic transitions in single crystals: A new molecular dynamics method. *J. Appl. Phys.* **52**, 7182–7190 (1981).
65. Wassenaar, T. A., Ingólfsson, H. I., Böckmann, R. A., Tieleman, D. P. & Marrink, S. J. Computational Lipidomics with insane: A Versatile Tool for Generating Custom Membranes for Molecular

Simulations. *J. Chem. Theory Comput.* **11**, 2144–2155 (2015).

66. Vickery, O. N. & Stansfeld, P. J. CG2AT2: an Enhanced Fragment-Based Approach for Serial Multi-scale Molecular Dynamics Simulations. *J. Chem. Theory Comput.* **17**, 6472–6482 (2021).
67. Bussi, G., Donadio, D. & Parrinello, M. Canonical sampling through velocity rescaling. *J. Chem. Phys.* **126**, 014101 (2007).
68. Essmann, U. *et al.* A smooth particle mesh Ewald method. *J. Chem. Phys.* **103**, 8577–8593 (1995).
69. Hess, B., Bekker, H., Berendsen, H. J. C. & Fraaije, J. G. E. M. LINCS: A linear constraint solver for molecular simulations. *J. Comput. Chem.* **18**, 1463–1472 (1997).
70. Michaud-Agrawal, N., Denning, E. J., Woolf, T. B. & Beckstein, O. MDAnalysis: A toolkit for the analysis of molecular dynamics simulations. *J. Comput. Chem.* **32**, 2319–2327 (2011).
71. Clark, J. *et al.* Quantification of PtdInsP3 molecular species in cells and tissues by mass spectrometry. *Nat Methods* **8**, 267–272 (2011).
72. Thibault, B. *et al.* Pancreatic cancer intrinsic PI3Kα activity accelerates metastasis and rewires macrophage component. *Embo Mol Med* e13502 (2021) doi:10.15252/emmm.202013502.

Figures

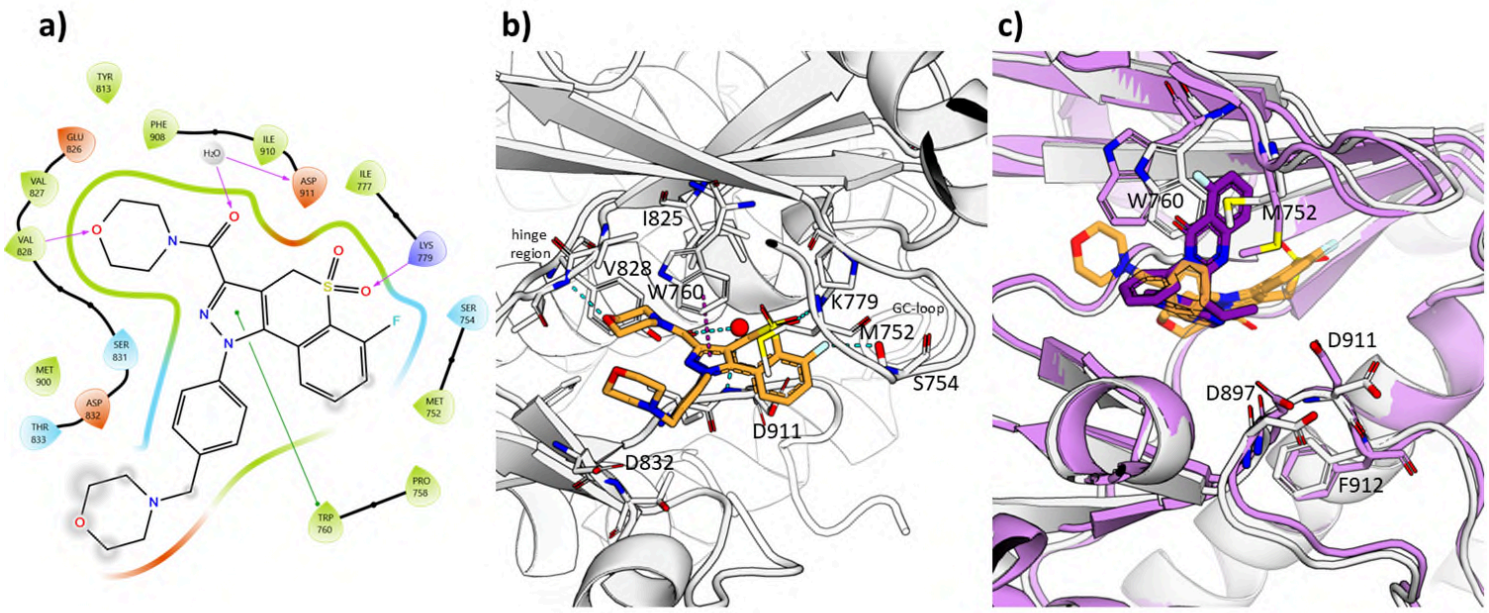


Figure 1

a Binding interactions of roginolisib within the protein active site. Roginolisib forms hydrogen bonds with V828 and K779, a solvent-mediated hydrogen bond with D911, and π-π stacking with W760. **b** Crystal structure of human PI3Kδ in complex with roginolisib (orange), solved at 2.75 Å resolution (PDB-ID: 9T07). Key interactions include hydrogen bonds (dashed cyan lines) with V828 (hinge), K779, S754 (via

aromatic fluorine), and the backbone NH of D911 (mediated by a water molecule), as well as π-π-interactions (dashed magenta line) with W760. **c**Superimposition of human PI3Kδ (grey)/roginolisib (orange) (PDB-ID: 9T07) and murine PI3Kδ/idelalisib (PDB-ID: 4XE0, purple) highlights the distinct binding mode of idelalisib, which targets the lipophilic pocket between M752 and W760 and the different orientations of D897 and D911 in both structures.

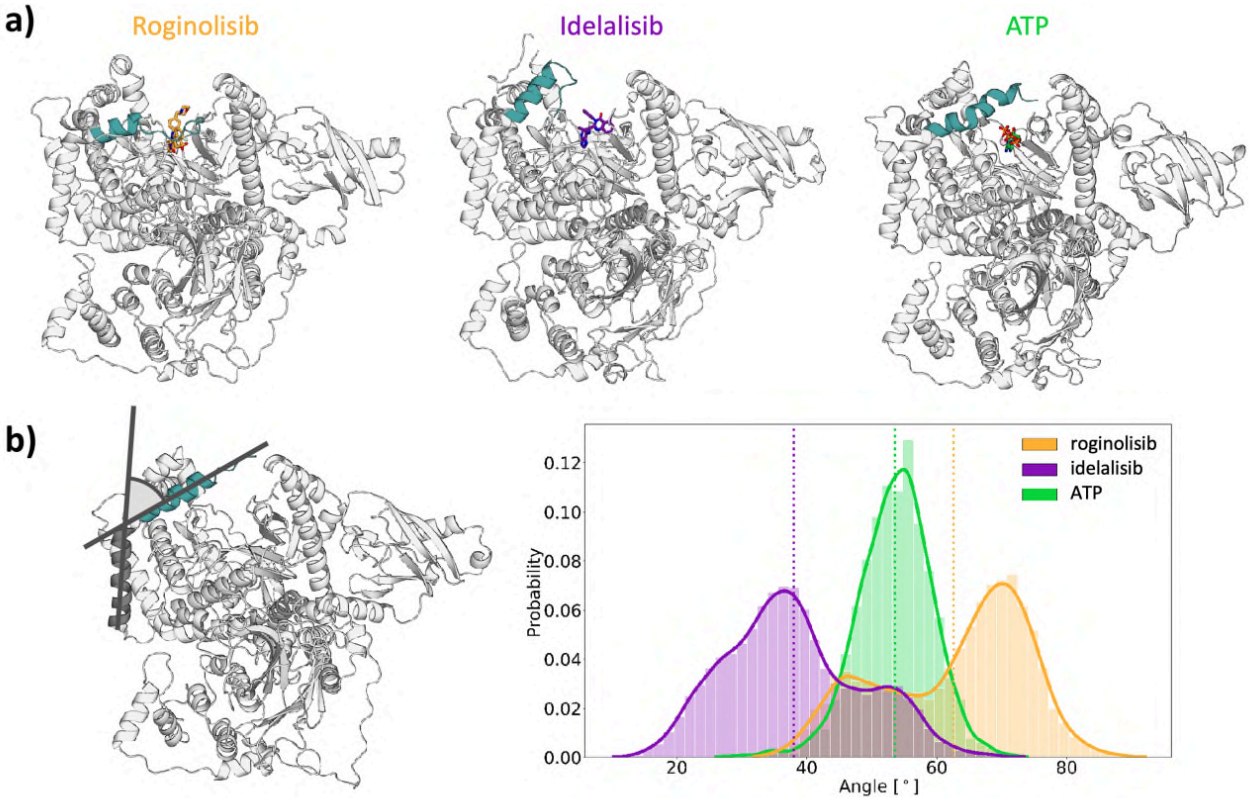


Figure 2

Difference in angle between PI3Kδ helix kα11 and the C-terminal helix kα12 in the presence of alternative bound ligands. **a** Representative simulation snapshots of roginolisib- (orange), idelalisib- (purple) and ATP- (green) bound structures with the C-terminal kα12 helix highlighted in teal. **b** Probability distribution of the angle formed between helix kα11 (grey) and kα12 (teal) across five replicates (n=5). The dotted lines represent the mean angle, corresponding to (62 ± 12) in the presence of roginolisib, (38 ± 11) with idelalisib and (54 ± 6) with ATP (mean ± SD in degrees).

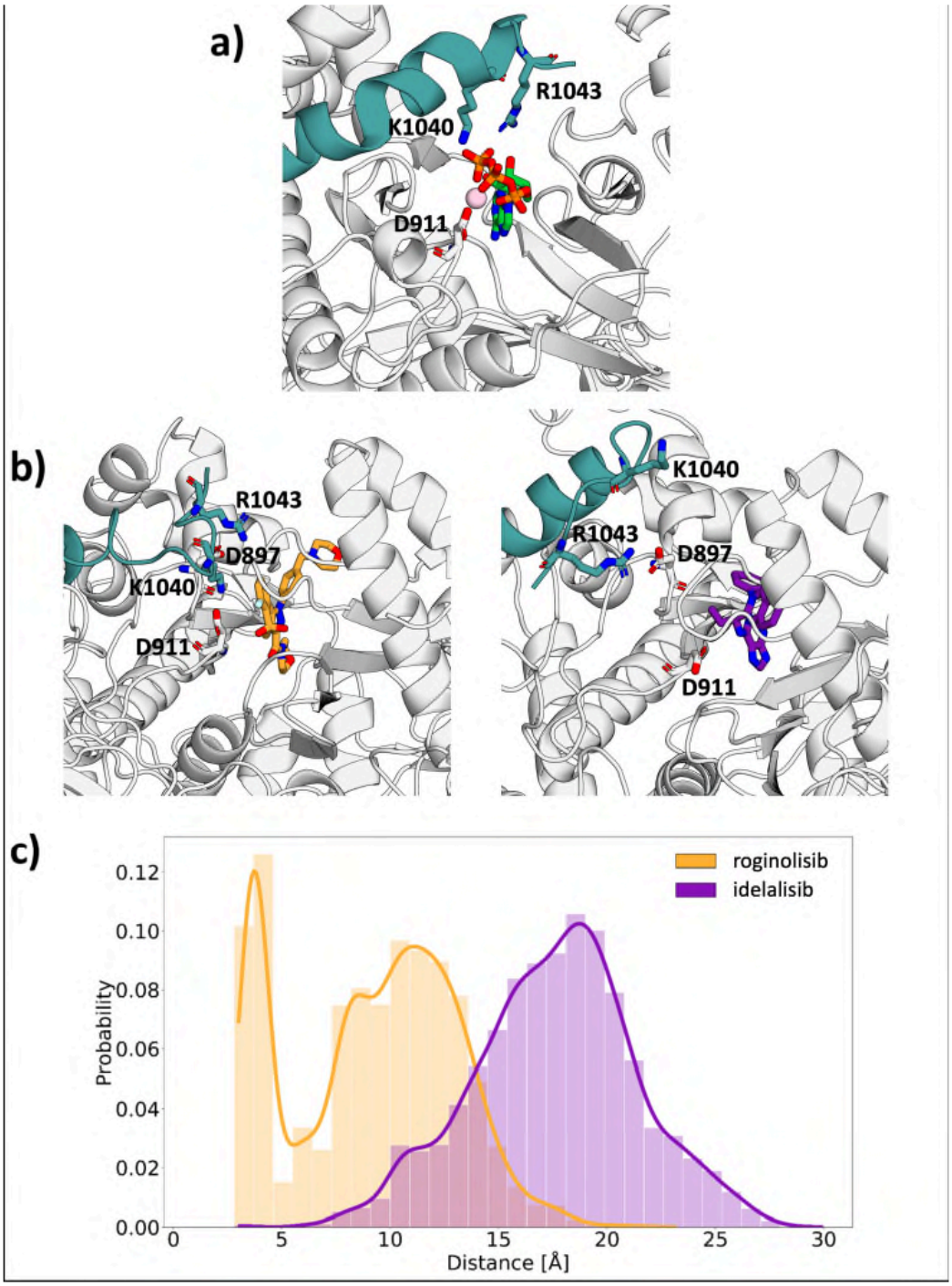


Figure 3

Specific interactions formed by basic residues of C-terminal kα12 helix in the presence of different ligands. **a** Close-up view of the ATP (green) binding site in a representative simulation snapshot, with the C-terminal helix kα12 highlighted in teal. Basic C-terminal helix residues Lys1040 and Arg1043, shown as sticks, interact with the γ-phosphate of ATP, with Asp911 of the DFG motif coordinating the magnesium ion (pink). **b** (left) Binding site of roginolisib (orange), where Lys1040 and Arg1043 form interactions with

Asp897 and Asp911. The positioning and conformation of roginolisib leads to a configuration of Asp911 that is oriented towards the C-terminal helix. (right). The idelalisib (purple) binding site. Arg1043 forms interaction with Asp897, with no interactions between Lys1040 and Asp911. **c** Probability distribution of the distance between the side-chain nitrogen atom of Lys1040 and carboxyl carbon of Asp911 across replicates (n=5), excluding the first 500 ns as equilibration time.

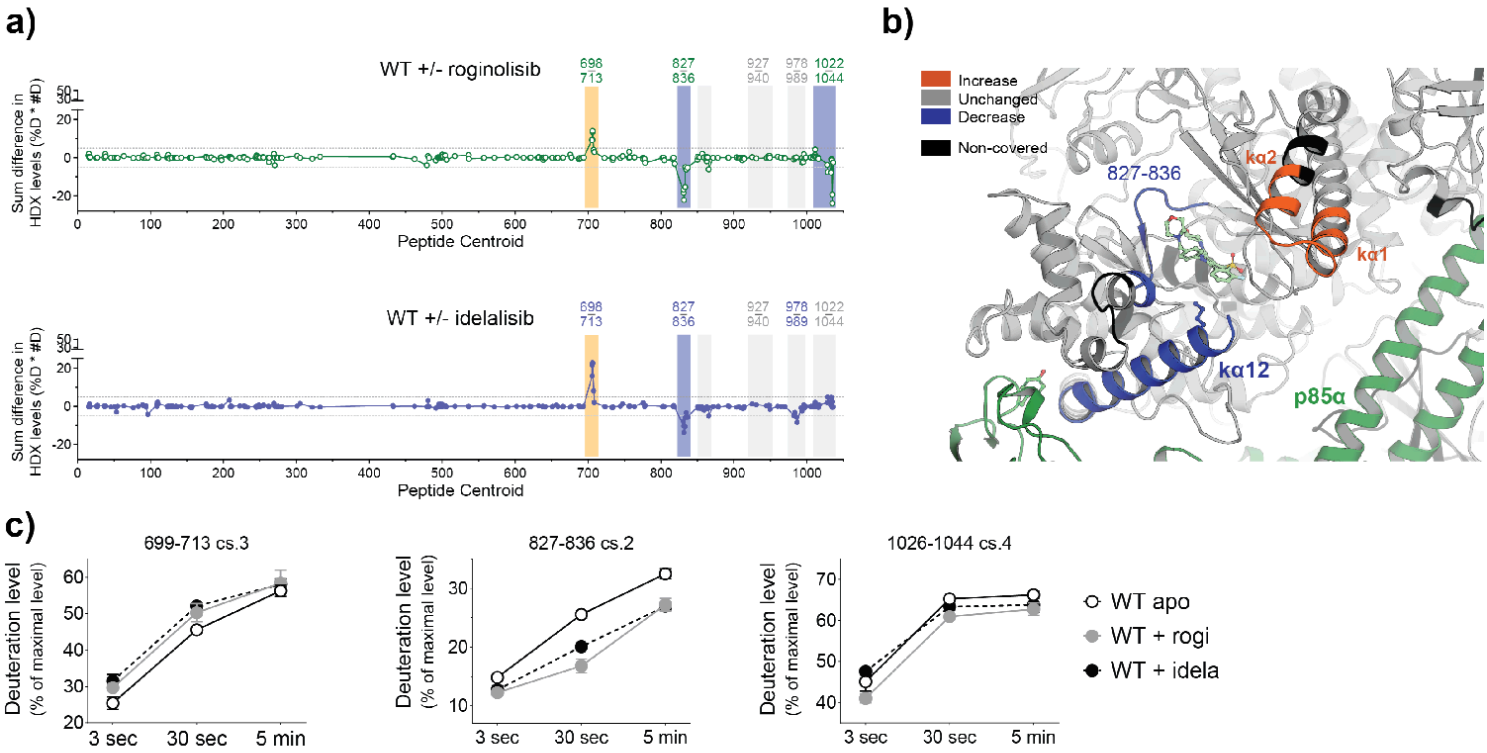


Figure 4

Identification of conformational changes on p110δ triggered by roginolisib and idelalisib binding to the p110δ/p85α complex using HDX-MS **a** Comparison of the H/D exchange rate of p110δ peptide between the apo p110δ/p85α heterodimer and roginolisib-bound complex (top) and idelalisib-bound complex (bottom). Each dot depicts a peptide, positioned based on the central amino acid (centroid). The sum of deuteron differences (Δ#D) multiplied by the sum of percentage differences (Δ%D) across all deuteration times is calculated and plotted on the y-axis. Regions showing significant difference in deuterium exchange (defined as Δ#D * Δ%D < 5) are coloured on the graph in orange (deprotection) or blue (protection) **b** Model of p110δ/p85α heterodimer bound to roginolisib highlighting regions to be differentially deuterated upon roginolisib binding (colour as shown in the legend). The p85α regulatory subunit is shown in green. **c** Uptake plots of a representative selection of p110δ peptides showing deuterium incorporation at three deuteration times for each of the studied conditions (WT p110α/p85α heterodimer in i) apo state; ii) when bound to roginolisib and iii) when bound to idelalisib). Data are shown as percentage deuteration (mean ± SD, n=3). cs = charge state.

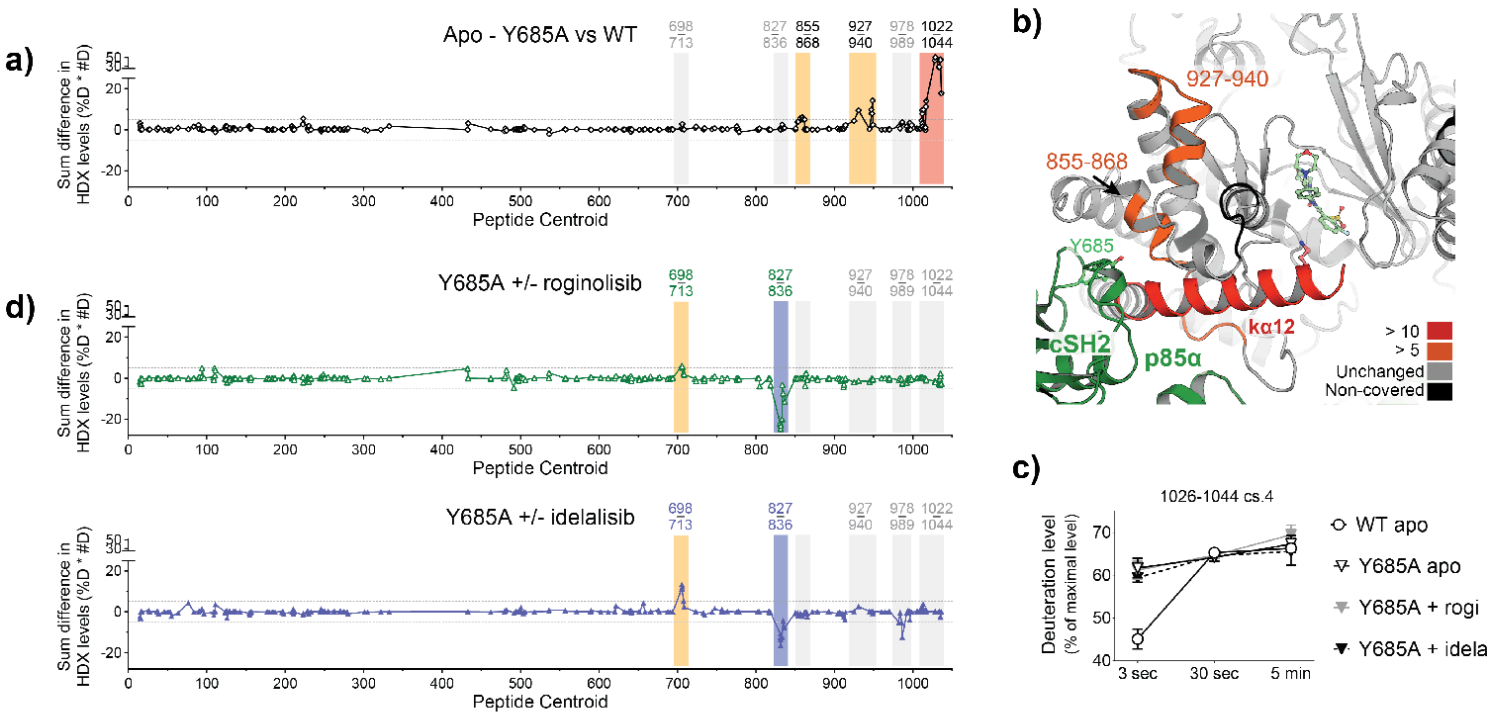


Figure 5

Roginolisib binding to activated p110δ/p85α-Y685A does not protect helix kα12 from exchange **a** Comparison of H/D exchange rates in p110δ peptides between WT and Y685A PI3Kδ. Each dot depicts a peptide, positioned based on the central amino acid (centroid). The sum of deuteron differences (Δ#D) multiplied by the sum of percentage differences (Δ%D) across all deuteration times is calculated and plotted on the y-axis. Regions showing significant difference in deuterium exchange (defined as Δ#D * Δ%D < 5) are coloured on the graph in orange (deprotection >5), red (deprotection >10) or blue (protection) **b**Mapping of regions affected by the p85α-Y685A mutation within p110δ. Colouring according to the legend. Roginolisib is shown to indicate the inhibitor binding site. The p85α regulatory subunit is coloured in green **c** Uptake plots of the p110δ peptide 1026-1044 showing deuterium incorporation at three deuteration times for each of the studied conditions (WT p110α/p85α heterodimer in i) apo state ; ii) Y685A heterodimer in apo state, ii) Y685A heterodimer in complex with roginolisib and iv) Y685A heterodimer when bound to idelalisib). Data are shown as percentage deuteration (mean ± SD, n=3). cs = charge state. (d) Comparison of H/D exchange rates in the p110δ peptides between apo and roginolisib (top) and idelalisib bound (bottom) p110δ/p85α-Y685A heterodimer. Data shown as in panel **a**

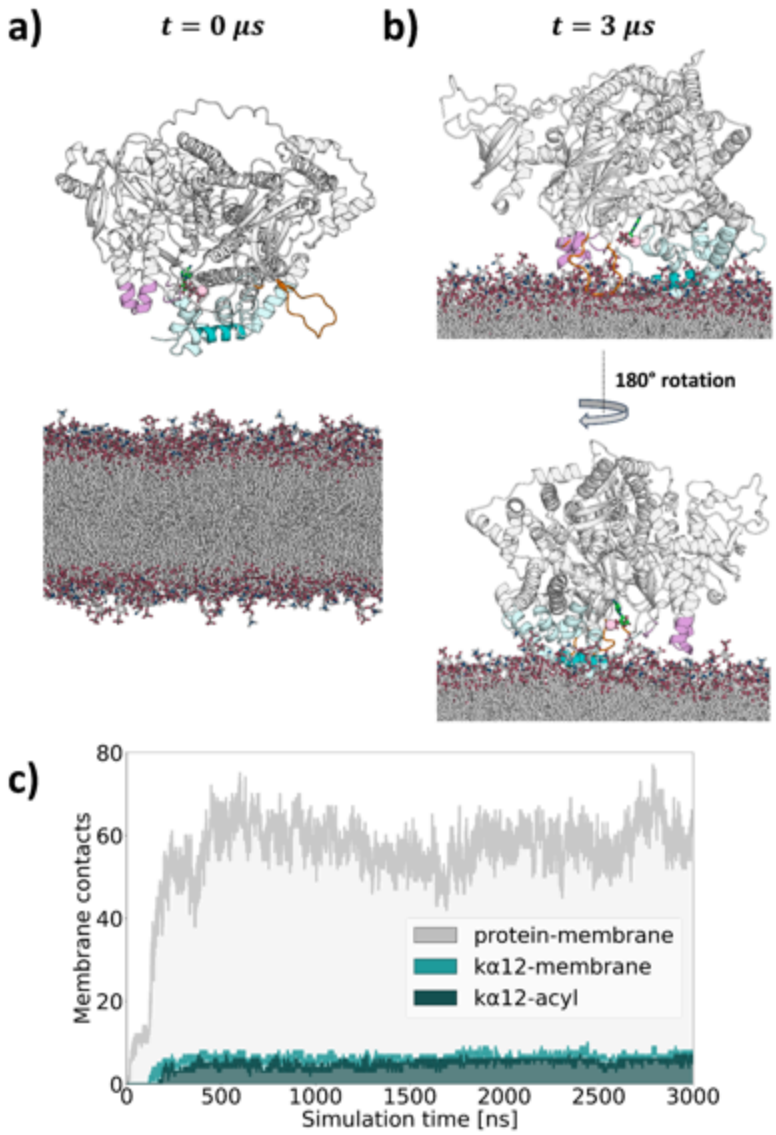


Figure 6

Protein-membrane association reveals key domains involved in membrane-bound/active conformation of PI3Kδ: C2 domain (orange), N-lobe (purple), C-lobe (light blue). Regions of these domains forming contact with membrane are coloured. kα12 is highlighted in teal. Membrane lipids are displayed in licorice with light grey coloured tails and dark grey phosphorus atoms. **a** Molecular graphic of initial simulation frame. The distance between protein and membrane is 2 nm and the structure is oriented in a way in which activation is suggested [15,30,31,44]. **b** Molecular graphics of final simulation frame at 3 μs show active PI3Kδ conformation upon membrane binding. Upper graphic shows deep insertion of loop of C2 domain which includes 9 basic residues. Lower graphic shows deep insertion of kα12 helix of C-lobe. **c** Number of contacts formed by entire protein (grey) and kα12 (teal) over time depicts association process and embedding into acyl of kα12 helix at 190 ns. The first made contact is at ~20 ns by the C2 domain loop and the loop's insertion is identifiable in the formation of the first elevation of up to 13

residues in contact with membrane until 120 ns before other regions of the protein begin interacting with membrane lipids.

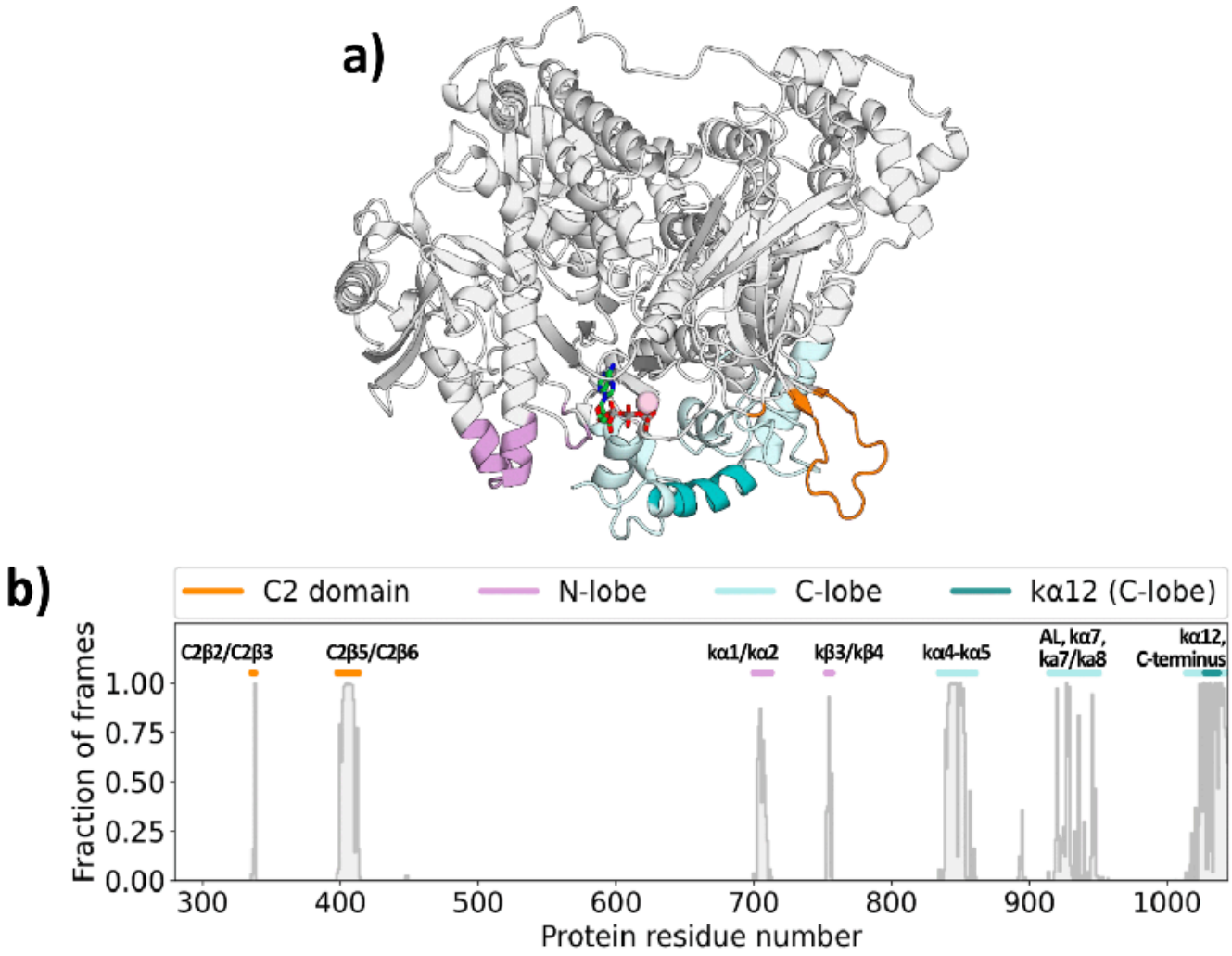


Figure 7

Regions forming contact to membrane during activation. **a** Molecular graphics of ATP·Mg^{2+}-bound PI3Kδ with regions forming contact to membrane highlighted: C2 domain (orange), N-lobe (purple), C-lobe (light blue). kα12 is highlighted in dark teal. **b** Protein membrane contact map strongly agrees with regions to be in contact with membrane discovered through HDX experiments [15]. A "/" separating two secondary structure elements stands for the hinge between those, whereas "-" stands for both of them including the hinge between. "AL" is the Activation Loop. The map reveals three major regions forming large contacts with membrane: the large loop between C2β5 and C2β6, parts of the helices kα4 and kα5, and kα12 plus the C-terminus.

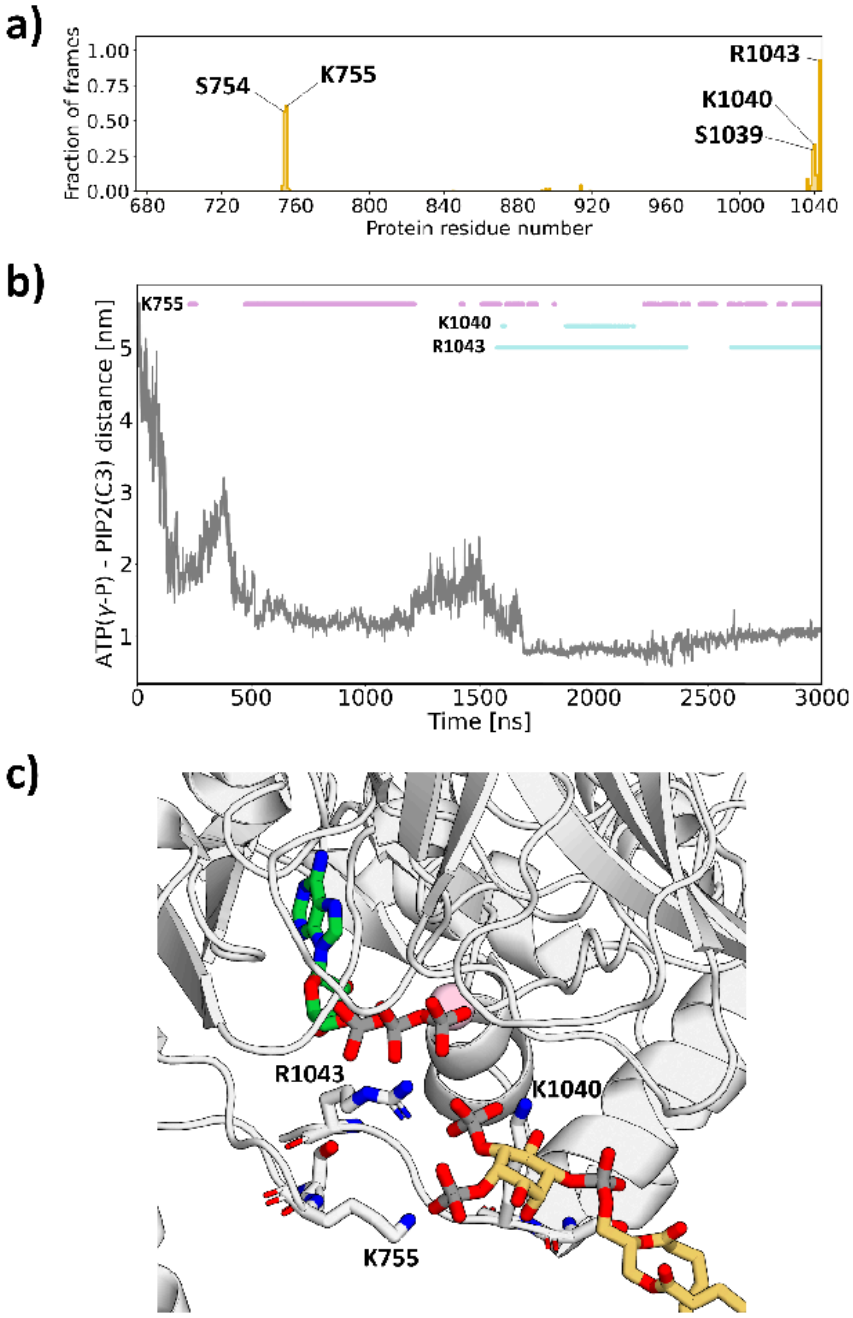


Figure 8

Basic residues of PI3Kδ interact with PIP2 forming an active compound. **a** Protein-PIP2 contact map reveals residues directly stabilising the active compound. Key residues are the basic residues Lys1040 and Arg1043 of the C-terminus and Lys755 of the N-lobe. Residues within 4 Å of the PIP2 lipid were counted. In addition, the contact map reveals Ser1039 to be in close proximity to the lipid facilitating reports on autophosphorylation of the residue to impact kinase activity[45]. **b** Distance between the γ-

phosphate of ATP and C3 of the inositol ring of the PIP2 lipid (grey) which is target for the phosphorylation depicts the insertion process of PIP2 into the active site. The first persistent contact is formed by Lys755 (purple) and both phosphate groups of PIP2 at ~500 ns. Stable interactions between PIP2 and the basic C-Terminus residues (light blue) follow at 1575 ns after guidance into the active site by Lys755 forming the phosphorylation competent active site. The top bars were created by adding a point at every frame in which the residues were within 4 Å of PIP2's 5-phosphate. **c** Simulation snapshot of phosphorylation competent site at 3 us. ATP (green), PIP2 (yellow) and the active compound stabilizing residues are shown as sticks and the magnesium ion is shown as a bead (pink).

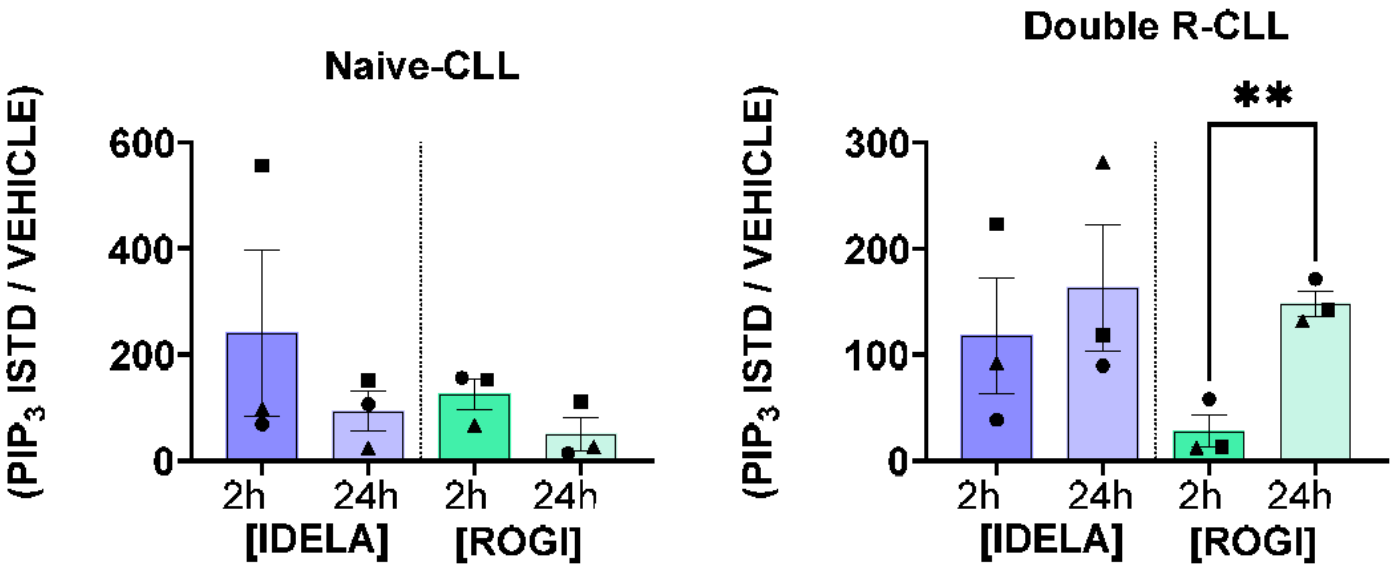


Figure 9

Lipidomic profiling of phosphoinositide molecular species in circulating tumor cells (CTCs) from CLL patients using LC-MS and TMS-derivatization for detection of PIP_3. CTCs were isolated from CLL patient (naïve of treatment or double refractory) and treated with vehicle, idelalisib (IDELA – 0.5μM) or roginolisib (ROGI-0.5μM) followed by lipid extraction using chloroform/methanol solvent, addition of internal standards (ISTD) for normalization, and derivatization with TMS-diazo-methane to enhance detection sensitivity. A tendency to a decrease of PIP3 level was observed in naïve-CLL patients at 2h and 24h in IDELA and ROGI-treated CTCs compared to VEHICLE. However, one patient (square) presented a peak of PIP3 production after 2h of IDELA treatment. Robust and significant inhibition of PIP3 was observed in all three double-refractory CLL CTCs treated with low doses of roginolisib for 2 hours, whereas two double-refractory patient (square, triangle) presented a peak of PIP3 production after 2h or 24h of IDELA treatment, respectively. Of note, and contrary to naïve patients, PIP3 levels in double-refractory were increased at the 24h time point with both inhibitors. Data are presented as % of VEHICLE.

Each symbol represents a patient, to analyse time course evolution of each of them. Mean ± SEM. ANOVA one-way test; *, p<0.05. Only statistically different p-values are shown.

Supplementary Files

This is a list of supplementary files associated with this preprint. Click to download.

- SupplementaryFigureLegends.docx
- SupplementaryTablesS1andS2.docx
- SupplementaryHDXTablesS3S4andS5.xlsx
- FiguresSupplementary.pptx
- MolecularDynamicsSimulationsChecklist176538661875.docx
- D1292151460valdataP1.xml.xml
- D1292151460valdataP1.cif.txt
- PI3KdeltaIOA288PDBfinal.txt
- nrreportingsummaryioamd.pdf
- D1292151471valdataP1.cif.txt
- D1292151460valreportfullP1.pdf.pdf
- D1292151460valreportwwpdbfofcedmapcoefP1.cif.txt
- PI3KdeltaRoginolisibPDBfinal.txt
- D1292151460valreportwwpdb2fofcedmapcoefP1.cif.txt
- D1292151471valreportwwpdbfofcedmapcoefP1.cif.txt
- D1292151471modelreviewP1.cif
- D1292151471valreportfullP1.pdf.pdf
- D1292151471valreportwwpdb2fofcedmapcoefP1.cif.txt